BINDING FREE ENERGY CALCULATION VIA MOLECULAR DYNAMICS SIMULATIONS FOR A miRNA:mRNA INTERACTION

G. Paciello, A. Acquaviva, E. Ficarra, M. A. Deriu, A. Grosso and E. Macii
Dep.of Control and Computer Engineering and Dep.of Mechanics, Politecnico di Torino
C.so Duca degli Abruzzi 24, Torino, Italy

Keywords: miRNA, Molecular dynamics, Thermodynamic integration.

Abstract: In this paper we present a methodology to evaluate the binding free energy of a miRNA-mRNA complex through Molecular Dynamics-Thermodynamic Integration simulations. We applied our method on the $C-elegans$ let-7 miRNA:lin-41 mRNA complex, known to be a validate miRNA:mRNA interaction, in order to evaluate the energetic stability of the structure. The methodology has been designed to face the various challenges of nucleic acid simulations and binding free energy computations and to allow an optimal trade-off between accuracy and computational cost.

1 INTRODUCTION

MicroRNAs (miRNAs) are endogenously produced $21 \div 23$-nt long riboregulators implicated in the control of biological processes such as differentiation, cell proliferation and developmental timing(Bartel, 2004)(Cevec et al., 2008). MiRNAs' target prediction is an interesting field of research widely investigated in the last years. Currently almost all the existing miRNAs' target prediction algorithms consider only general principles based on secondary structure analyses.

In the present work, we propose a study of the energetic stability of a specific experimentally validated interaction(Vella et al., 2004), that is the bound between $C-elegans$ let-7 miRNA fragment and its complementary site *LCS*2 in the $3'$ UTR of the lin-41 mRNA(Cevec et al., 2008), by calculating their binding free energy via Molecular Dynamics (MD)-Thermodynamic Integration (TI) simulations.

The contribution of this work is twofold. First, we devise a methodology for the computation of the free energy of this interesting class of RNA strands, also taking into account the computational costs. Second, thanks to the MD simulations, we highlighted the relevance of tridimensional structure informations on the free energy result.

2 MATERIALS AND METHODS

2.1 System Set-up

The original NMR let-7:lin-41 atomic structure(Cevec et al., 2008) was taken from the Protein Data Bank (PDB) with accession code 2JXV and then modified to better mould the interaction between miRNA and mRNA pointed out in nature(Vella et al., 2004).

The secondary structure so obtained is shown in Figure 1.

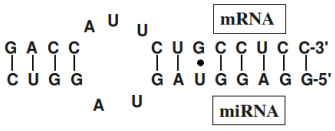

Figure 1: let-7 miRNA:lin-41 mRNA modified model. The dot represents a wobble base pair.

The modified complex was solvated in a cubic box with 12000 TIP4P water molecules to avoid distortions(Cheatham, 2004) and then its negative net charge neutralized with 27 sodium ions. The coordinates were optimized via 3 ps *steepest descendent* energy minimization, after which an *all atom position restrained* simulation for 5 ps under a constant force of 1000 $kJmol^{-1}nm^{-2}$ was carried out. All the simulations were performed using the ffamber94 Force Field(Cornell et al., 1995) that we integrated in Gro-

Paciello G., Acquaviva A., Ficarra E., A. Deriu M., Grosso A. and Macii E..
BINDING FREE ENERGY CALCULATION VIA MOLECULAR DYNAMICS SIMULATIONS FOR A miRNA:mRNA INTERACTION.
DOI: 10.5220/0003167703180321
In *Proceedings of the International Conference on Bioinformatics Models, Methods and Algorithms* (BIOINFORMATICS-2011), pages 318-321
ISBN: 978-989-8425-36-2

macs 4.0.5 distribution(Van Der Spoel et al., 2005).

2.2 Molecular Dynamics Simulations

A preliminary set of MD simulations was conducted to check the conformational stability of the molecular system and to select the best simulation parameters to adopt in the subsequent free energy simulations. Due to the well known helix shape modifications(Pan and Mackerell, 2003), the first and the last nucleotides of both RNA chains were restrained with a force constant of $1000 kJmol^{-1}nm^{-2}$. The temperature was maintained constant at $310K$ and all bonds were kept rigid thanks to the LINCS Algorithm. Non bonded interactions were calculated using a neighbor list updated every 5 time steps. Cut-off distance for short-range interactions was set at $1.2nm$. Fast Particle-Mesh Ewald electrostatics (*PME*) in all the three dimensions was used to calculate long-range electrostatic forces. The interpolation order for PME was set as cubic whereas the relative strength of Ewald-shifted direct potential at Coulomb distance at 10^{-5}. A leap-frog algorithm was used for integrating Newton's equations of motion. Trajectory structures were saved at $0.1ps$ intervals from a $1ns$ and a $10ns$ long molecular dynamics simulations.

2.3 Free Energy Calculations

Thermodynamic-Integration (TI) approach was used to calculate the binding free energy. The TI technique allows to obtain the free energy difference ΔG between two states of a system, A described by a Hamiltonian $H(\lambda = 0) = H_A$ and B defined by a Hamiltonian $H(\lambda = 1) = H_B$, by changing from A to B state the interaction parameters that define the Hamiltonian H as a function of a coupling parameter λ as showed in Eq. 1.

$$\Delta G_{BA} = G_B - G_A = \int_0^1 \frac{dG(\lambda)}{d\lambda} d\lambda = \int_0^1 \langle \frac{dH(\lambda)}{d\lambda} \rangle_\lambda d\lambda \quad (1)$$

The thermodynamic cycle implemented to achieve the desired binding free energy value is reported in Figure 2(Lawrenz et al., 2009).
In order to achieve the conditions described by the thermodynamic cycle, the B state of the system was opportunely edited during the simulations. At any intermediate state the Hamiltonian of the system was defined by Eq. 2.

$$H(\lambda) = (1-\lambda)H_A + \lambda H_B \quad (2)$$

Regarding Eq. 2, the ensemble averages of the derivative of the Hamiltonian were calculated via $1ns$ long constrained MD simulations at the constant pressure of $1atm$. The averages of the derivatives, obtained from the simulations, were then integrated giving rise to ΔG_1 (Figure 2) and ΔG_2 (Figure 2). The binding free energy was then calculated by subtracting the first quantity to the second as synthesized in Figure 2.

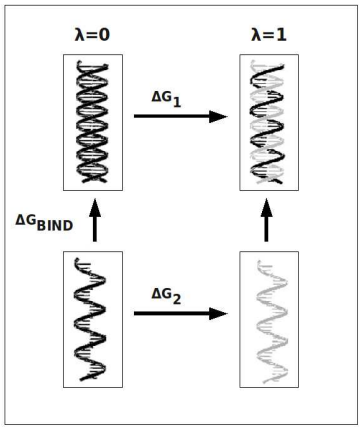

$$\Delta G_{BIND} = \Delta G_2 - \Delta G_1$$

Figure 2: Thermodynamic cycle used in binding free energy calculations. The two branches of the cycle have to be considered in order to obtain the free energy of binding between the ligand, mRNA, and the receptor miRNA.

3 RESULTS AND DISCUSSION

3.1 Molecular Dynamics

The stability of let-7:lin-41 complex, known to be strictly depending on several elements(Cheatham, 2004), was evaluated via the atom positional-RMSD analysis in the unconstrained MD trajectory structures from the initial molecular configuration. Let-7 miRNA, called 'Chain A', showed an average RMSD value of $0.281nm$ and a maximum RMSD value of $0.421nm$ after about $887ps$ of simulation. Lin-41 mRNA, called 'Chain B' presents, instead, a higher RMSD mean value of about $0.389nm$, and a remarkable deviation from the initial trajectory in the first part of the run.

To maintain the original helix shape during the run the atomic fluctuations of about 30 atoms (one nucleotide) at the beginning and at the end of the strands were limited: In this manner the RMSD average value for Chain A is $0.136nm$ whereas for Chain B is $0.167nm$. The achieved stability of the complex was analyzed also via a $10ns$ long simulation. In this case the maximum RMSD value obtained is $0.214ns$ after $5090ps$ of running. The choice to adopt re-

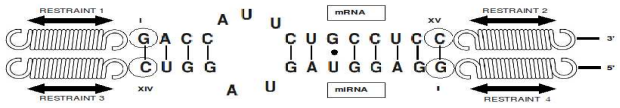

(a)

RESTRAINT	ELASTIC CONSTANT VALUE	RESTRAINED CHAIN	RESTRAINED NUCLEOTIDE	BIOLOGICAL JUSTIFICATION
RESTRAINT 1	1000kJ/mol·nm²	mRNA	I	PRESENCE OF THOUSANDS OF NUCLEOTIDES IN 5' mRNA DIRECTION SURROUNDING LCS2 SITE
RESTRAINT 2	1000kJ/mol·nm²	mRNA	XV	PRESENCE OF THOUSANDS OF NUCLEOTIDES IN 3' mRNA DIRECTION SURROUNDING LCS2 SITE
RESTRAINT 3	1000kJ/mol·nm²	miRNA	XIV	PRESENCE OF THE RNP COMPLEX BOUND TO THE 3'-miRNA END
RESTRAINT 4	1000kJ/mol·nm²	miRNA	I	PRESENCE OF THE RNP COMPLEX BOUND TO THE OPPOSITE 3' miRNA END AND NEIGHBOR NUCLEOTIDES IN 3'-miRNA DIRECTION

(b)

Figure 3: Model and explanation of the molecular system during the constrained simulation. In Subfigure (a) is reported a scheme of the constrained molecular complex and in Subfigure (b) the summarize of the restraints applied.

straints, sketched and summarized in Figure 3 (a) and (b), was considered plausible by taking into account previous biological researches(Schwarz and Zamore, 2002)(Vella et al., 2004).

3.2 Free Energy Calculations

The binding free energy values were obtained by starting from a number of lambda set to 11 and by incrementing it progressively until (for a fixed number of lambda) the percentage error of the ensamble averages of the derivative of the Hamiltonian between two successive lambda values was inferior to a threshold set to 4% with respect to the total variation between $\lambda = 0$ and $\lambda = 1$.

The criterion was satisfied for both ligand and complex with 60 lambda values. In this sampling conditions, the free energy for the branch relative to the complex was equal to $4043,57 kcal/mol$ whereas for the ligand it was $3939,32 kcal/mol$. As such, the final binding free energy value obtained was $-104,25 kcal/mol$. We noticed however that starting from 51 lambda values the error is clearly reaching an asintotic behaviour with percentage errors around 2%.

This aspect was further investigated by considering the accuracy of the free energy results obtained with respect to the error achieved using 60 lambda values, for which the threshold error criterion is satisfied: We noticed that a very good accuracy is reached already with 19 lambda, the percentage error is about 7% and a further improvement is obtained with 51 lambda, the error is here about 0.25%.

3.3 Scalability Analysis

In the following we report about the characterization of the stability of the binding free energy computations on a Symmetric Multiprocessing (SMP) architecture, namely a 4+4 Intel(R) Core(TM) i7 CPUs 920 @ 2.67GHz machine. The simulations for various lambdas were implemented as independent processes. The experiments were conducted using the set up of the TI-MD simulations previously discussed, but with a length reduced to 5ps since by profiling the short and long simulations we observed the same characteristics in terms of system resource utilization (i.e. percentage of memory and cache accesses). We run 2, 4, 8, 12, 16, 24, 32 and 64 parallel simulations during which the average percentage CPU user utilization for the processes was recorded by taking advantage of the command *pidstat* of the *Sysstat* utilities. We will report here only the obtained CPU user utilization statistics, because the system utilization for the processes was found to be negligible. As it is shown by trace 'I' of Figure 4, the real trend of the average CPU utilization for the processes is very different from the ideal one of Figure 4 trace 'II', obtained by assuming a perfect independence between processes, that is the simulation time is independent from the number of lambdas: Even if we increase the number of simulations and thus the workload imposed to the system, the simulation time remains constant until the number of CPU is larger or equal to the number of processes. Then it increases in a linear way. Trace 'I' is far from the ideal behavior, as the simulation time increases as a function of lambda. This is mainly due to two effects. The first effect is the impact of memory congestion. Indeed, even if the processes do not communicate or use shared memory

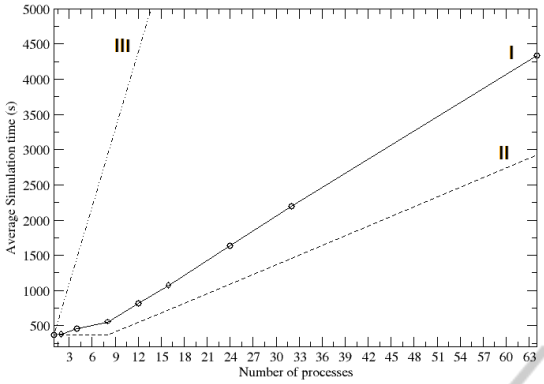

Figure 4: Trend of the simulation time at the increasing of the running processes. Trace 'I' and 'II' are respectively the real and the ideal trend for the simulation time obtained by running an increasing number of parallel processes, whereas trace 'III' is that relative to an increasing number of serial processes. The cycles on Trace 'I' mark the number of processes for which the test have been made.

regions, there is a considerable contention for access to the L2 cache and the main memory. The latter arises when the number of processes overcomes the number of available CPUs. Indeed, it can be observed that trace 'I' is characterized by two different trends. The first one, from 1 to 8 lambda, where only the memory contention contributes. The second, from 8 to 64 lambda, where the context switch and process migration overheads are also present, leading to an increasing slope of the curve. The utilization is almost 100% before 8 lambda and decreases after 8 lambda, where each process has to share the CPU with others. It is worth nothing however that besides the overhead discussed, the parallelization is unquestionably more advantageous with respect to performing serial simulations, whose simulation times are reported in Trace 'III' of Figure 4. Overall, by putting together the accuracy results with the computation costs, we can conclude that a suitable trade-off between computation and accuracy can be set to 19 lambda.

4 CONCLUSIONS

The methodology presented in this paper has been designed to face the various challenges of nucleic acid simulations and binding free energy computations. First, the positioning of the restraints has been determined to overcome the stability problems due to the remarkable folding activity and the base pairs opening of the complex. As a results, we were finally able to perform MD simulations in stable conditions.

Second, the accuracy of the thermodynamic integration steps. On this concern, we studied the scalability of the thermodinamic integration to determine a reasonable trade-off between computation and accuracy. We shown that to achieve an error on the binding free energy computation lower than 4% we need to perform 60 parallel simulations. On the other side, a good trade-off between computation and accuracy is already reached using 19 parallel simulations.

REFERENCES

Bartel, D. P. (2004). MicroRNAs: Genomics, Biogenesis, Mechanism, and Function. *Cell*.

Cevec, M., Thibaudeau, C., and Plavec, J. (2008). Solucttione structure of a let-7 miRNA:lin41 mRNA complex from C.elegans. *Nucleic Acids Research*.

Cheatham, T. E. (2004). Simulation and modelling of nucleic acid structure, dynamics and interactions. *Current Opinion in Structural Biology*.

Cornell, W. D., Cieplak, P., Bayly, C. I., Gould, I. R., Merz, K. M., Ferguson, D. M., Spellmeyer, D. C., Fox, T., Caldwell, J. W., and Kollman, P. A. (1995). A second generation force field for the simulation of proteins, nucleic acids, and organic molecules. *J. Am. Chem. Soc.*

Lawrenz, M., Baron, R., and McCammon, J. A. (2009). Independent-trajectories thermodynamic-integration free-energy changes for biomolecular system: Determinants of N5HN1 Avian Influenza Virus Neuraminidase Inhibition by Peramivir. *Journal of Chemical Theory and Computation*.

Pan, Y. and Mackerell, A. D. (2003). Altered structural fluctuations in duplex RNA versus DNA: a conformational switch involving base pair opening. *Nucleic Acids Research*.

Schwarz, D. S. and Zamore, P. D. (2002). Why do miRNAs live in the miRNP? *Genes e Development*.

Van Der Spoel, D., Lindahl, E., Hess, B., Groenhof, G., Mark, A. E., and Berendsen, H. J. C. (2005). GROMACS: Fast, flexible, and free. *Journal of computational chemistry*.

Vella, M. C., Reinert, K., and Slack, F. J. (2004). Architecture of a validate microRNA::target interaction. *Chemistry e Biology*.